Rock Mechanics and Rock Engineering (2020) 53:2233–2248
https://doi.org/10.1007/s00603-019-02027-9

ORIGINAL PAPER

Coupling Instability Mechanism and Joint Control Technology of Soft-Rock Roadway with a Buried Depth of 1336 m

Qinjian Zhan[1,2,3] · Xigui Zheng[1,3] · Jiping Du[1,3] · Tan Xiao[2]

Received: 31 March 2019 / Accepted: 26 November 2019 / Published online: 10 December 2019

Abstract

Based on the geological conditions of soft-rock roadway with a buried depth of 1336 m and the data that are achieved by various experimental methods, the multi-factor coupling analysis of the instability mechanism of soft-rock roadway is carried out through theoretical analysis and numerical simulation. Additionally, following the Nishihara model and Drucker–Prague's modification of Mohr–Coulomb yield condition, the stability control theory of soft-rock coal roadway is analyzed. By fully considering the bearing capacity of each supporting component, the original supporting structure is innovatively examined with crush tube, spherical tray, high-strength bar and steel strip to form a flexible and high-performance bolt supporting structure, and the stability control of 1336 m soft-rock coal roadway is also comprehended. Therefore, the studies have shown that the convergence trend of omnidirectional, strong rheological and large deformation constitutes the essential characteristics of deep soft-rock roadway deformation. The instability process of roadway surrounding rock is accompanied by "domino-effect" similar to that of multi-factor coupling. The irrational design of the support scheme and the destruction of the support structure are the external factors of this effect, although the prominent contradiction between high in-situ stress and the weak bearing capacity of the deep degraded rock mass is the internal factors of this effect. Similarly, the engineering practice and observation data of the new scheme have shown that the deformation coordination of support components and the matching degree of bearing characteristics should be one of the main factors to be considered in the design of deep soft-rock roadway support, high elongation and multiple adjustable characteristics to adapt to the basic characteristics of deep soft-rock roadway deformation. Hence, the construction idea of the new scheme has contributed the satisfactory engineering significances and reference value for optimizing the stress environment of soft-rock roadway and further reducing the support cost.

Keywords Soft-rock coal roadway · Coupling analysis · Instability mechanism · Domino effect · Omnidirectional · Strong rheology

Abbreviations

NATM	New Austrian tunneling method
ASTM	American society for testing and materials
ISRM	International society for rock mechanics
CCNSCB	Cracked chevron-notched semi-circular bend
CCNBD	Cracked chevron-notched Brazilian disc

List of Symbols

H	Height of roadway
n	Assurance factor
a	Radius of roadway
p_{α}	Supporting intensity
G_1	Shear modulus
r	Depth of surrounding rock
S	Anchor row space
p	The axial force of anchor bolt
k	Stiffness of anchor bolt
Δu^r	Radial displacement of rock stratum
E	Elasticity modulus
M_{φ}	Friction angle-softening modulus
F	The normal yield of material under three-dimensional stress
$\langle F \rangle$	The normal yield of material under three-dimensional stress conditions
L	Roadway width

✉ Qinjian Zhan
zhanqinjian@126.com

[1] School of Mines, China University of Mining and Technology, Xuzhou 221116, China

[2] Architectural Engineering Institute, Guangdong University of Petrochemical Technology, Maoming 525000, China

[3] The State Key Laboratory for Geo Mechanics and Deep Underground Engineering, China University of Mining and Technology, Xuzhou 221116, China

$[r]$	The radius of loose surrounding rock
p_0	In-situ stress
G_1	Shear modulus
b	Bolt spacing
d	Thickness of the compression band
p^{r}	Pre-strength of anchor bolt
u	Surrounding rock displacement
v	Surrounding rock migration rate
A	Cross-sectional area
M_c	Viscosity-softening modulus
L_0	Supporting length

Greek Symbols

σ_ρ	The radial stress
σ_θ	Circumferential stress
$\sigma_{H\max}$	Maximum horizontal principal stress
$\sigma_{H\min}$	Minimum horizontal principal stress
σ_1	Maximum principal stress
σ_3	Minimum principal stress
σ_t	Tensile strength
σ_n	Normal stress
σ_c	Vertical principal stress
σ_c'	Residual cohesion
σ_r^e	Effective radial stress of the elastic–plastic boundary surface
$\tau_{\rho\theta}$	Shear stress
φ	Internal friction
φ'	The residual angle of internal friction
η_1	Proportional constant
ψ_1	Viscosity coefficient
ψ_2	Viscosity coefficient
μ	Poisson's ratio
$[\varepsilon]$	The critical strain of rock mass
ε	Linear strain
ε_e	Elastic linear strain

1 Introduction

The strong rheology (Zhang et al. 2018) and large deformation (Tan et al. 2015) have developed the main characteristics of deep soft-rock roadway deformation. Some countries closed all or part of the underground coal mines, due to their great mining depth and high costs (Kang 2014). In recent years, the stability control of soft-rock roadway has been studied extensively by various researchers from different countries such as America, Australia, Germany, Netherlands and China. The America and Australia have established advanced bolt-mesh-shotcrete technology for the stability control of surrounding rock (Shreedharan and Kulatilake 2016). According to the instability criterion of shear failure and transverse expansion theory, the anchor bolt was considered to be inevitable for providing shear strength and axial limitations of the rock mass (Frith et al. 2018; Kang et al. 2015). However, in Germany, Netherlands and other European countries (Zhao and Zhang 2017), adapt the stretchable U-steel for large section roadway and has used the significant supporting structure. Using U-steel between anchor bolt and backfilling is frequently appeared in the practice of deep roadway.

After many years of research and improvement, the new Austrian tunneling method (NATM) has become the prominent technique in China, which accounts for about 70%, even over 90% in a state-owned coal mine (Kang et al. 2011). Besides, joint support technology based on NATM has been widely used in soft-rock roadway including bolt-mesh-shotcrete, steel truss anchor and shotcrete, anchor belt rack, anchor spray rack, etc. (Lu et al. 2011; Zheng et al. 2013). As a further development of the joint support technology, as per the theory of bolt-shotcrete arc plate supporting, in the initial stage of roadway support, the flexible supporting structure was more competent than rigid support (Zhu and Ren 2019; Sun 2015). On the other hand, the theories like loosing circle of surrounding rock theory (Yu et al. 2016), supporting a theory of bearing ring and stress control theory (Shreedharan and Kulatilake 2016), mainly focused on the causes of roadway instability and support failure (Yu et al. 2015; Yang and Li 2012).

Keeping in view the above scenario, it is generally concluded that the joint support technology implies significant supporting effects (Feng et al. 2017). However, due to the complexity of stress environment (Wang et al. 2018), rock damage, lithologic deterioration and the contradiction between cost and safety, the blind empirical or the narrow pursuit of high strength support will lead to a vicious cycle of "destruction-restore-destruct". More seriously, the roadway collapse resulting in time-consuming, laborious and higher maintenance costs. Therefore, the ideal support system should be facing various challenges arising from different geological conditions, and also decreases the supporting charge. This requires the accomplishment of two necessary premises, one of which is the content of the above discussion, that is, to shape a sound support system and second is to develop the crack initiation. The basic research on rock fracture mechanics, such as propagation (Song et al. 2018), is because the calculation contains cracks, the structural integrity and collapse threshold of the discontinuous rock mass. It is not only a fascinating academic topic but also has essential significance in engineering practice. Accordingly, the exploration of rock mass damage, fracture and crack propagation has become one of the research focuses, and the test of rock fracture toughness values seems to carry more attention (Liu et al. 2018; Feng et al. 2018; Ghazvinian et al. 2013; Nazerigivi et al. 2018).

Since the 1960s, a largenumber of sample types and methods have been developed for testing the fracture toughness of rocks (Ghamgosar et al. 2017; Erarslan et al. 2014; Xu and Dai 2017; Erarslan and Williams 2012; Ghamgosar and Erarslan 2016; Serati et al. 2016). To facilitate the comparison

of experimental data and achieve the standardization of fracture toughness test, the corresponding measurement methods like the American Society for Materials and Testing (ASTM) and International Society of Rock Mechanics (ISRM) are conducted. These both methods have better consistency and comparability. Additionally, this indicates a great significance to establish a feasible and reasonable fracture toughness test system. Therefore, in view of the comparison, revision and improvement of different test methods, many researchers have conducted various studies. Studies have shown that, in addition to the testing methods, the measurement of fracture toughness is also affected by size effect (Aliha et al. 2012), confining pressure effect (Ghamgosar and Erarslan 2016), loading rate (Colussi et al. 2016), prefabricated crack size and style (Ayatollahi and Aliha 2004), loading method (Aliha and Bahmani 2017), rock material form (Ayatollahi and Varasteh 2017), test method (Ayatollahi et al. 2019), and loading equipment and other factors. Undoubtedly, many scholars have made outstanding contributions to the research of rock mass damage and crack propagation, and played a key role in promoting the experimental development of rock fracture mechanics.

The stressed environment of the deep roadway is complex, and the degraded rock mass often exhibits creep and even rheological conditions.

This paper is supported by data obtained from various empirical methods (including section convergence test, original rock stress test, borehole teat, and bearing characteristics analysis of failure components). Based on theoretical analysis, numerical simulation and other research methods, the multi-factor coupling analysis of instability mechanism of soft-rock coal roadway is carried out. The theoretical analysis of integrating stability control of soft-rock roadway,on the basis of fully considering the bearing capacity of each supporting component,renew the organic combination of crush tube, spherical tray, high-strength bar, steel strip and its applications are in practice. Hence, the results of numerical simulation and engineering practice show that the new support scheme optimizes the surrounding rock stress environment and comprehends the stability control of the soft-rock coal roadway. Furthermore, this study can provide valuable guidance and reference value for the stability control of soft-rock coal roadway.

2 Project Overview

2.1 Engineering Geology

The fourth level of Suncun Coal Mine refers to − 1100 m and the buried depth of transport roadway on working face-2423 with 1336 m. The average thickness of coal seam was 3.1 m, the bedding of coal seams was developed, and the part contains stratification or pseudo-roof was 0.10 to 0.3 m. The coal-measured strata belong to Shanxi formation of lower Permian of Paleozoic Permian. The roof was graded from medium-grained sandstone to fine sandstone or siltstone, and the floor was siltstone, which was well developed and contains pyroclastic fossils. As shown in Table 1, compared to the mechanical properties of rock stratum in shallow part, the rock masses in deep demonstrates the prominent deterioration characteristics.

2.2 Support and Deformation

Figure 1 shows the original support design of soft-rock coal roadway, the supporting system of the floor and roof was arranged by an asymmetric structure. The roadway was supported by the anchor-mesh structure. The metal mesh was located on the full section of roadway. The BHW-280-3.00 steel strip was placed between the anchor bolt and the metal mesh. A flat tray was made of 250 × 250 × 15 mm steel plate, and the type of capsule resin was ZΦ 23 × 500 mm. Similarly, the anchor bolt was made of left-hand twist threaded steel bars without longitudinal rib, the material of which was low-alloy high-strength structural steel (16 Mn), and 20 mm in diameter. Each anchor bolt was provided with two capsule resins, and the pre-strength of anchor bolt was 35 kN. The

Table 1 Physical and mechanical parameters of each rock stratum

Rock	Dry density/kg m^{-3}	Modulus of elasticity (static)/GPa	Modulus of elasticity (dynamic)/GPa	Shear modulus/GPa	Tensile strength/MPa	Poisson's ratio	Cohesion/MPa	Angle of internal friction/°
Sandstone	2550	8.17	11.16	8.2	2.93	0.23	1.63	42
Mudstone	2600	3.81	5.01	2.62	2.1	0.22	1.35	36
sandstone	2550	8.17	11.16	8.2	2.93	0.23	1.63	42
Siltstone	2620	12	16.56	10.5	3.58	0.24	1.97	40
4$^{\#}$coal	1475	5.12	6.86	4.14	0.69	0.25	1.08	28
Siltstone	2620	12	16.56	10.5	3.58	0.24	1.97	40
Fine sandstone	2650	13.36	18.47	5.26	3.28	0.24	1.76	46
Sandstone	2550	8.17	11.16	8.2	2.93	0.23	1.63	42

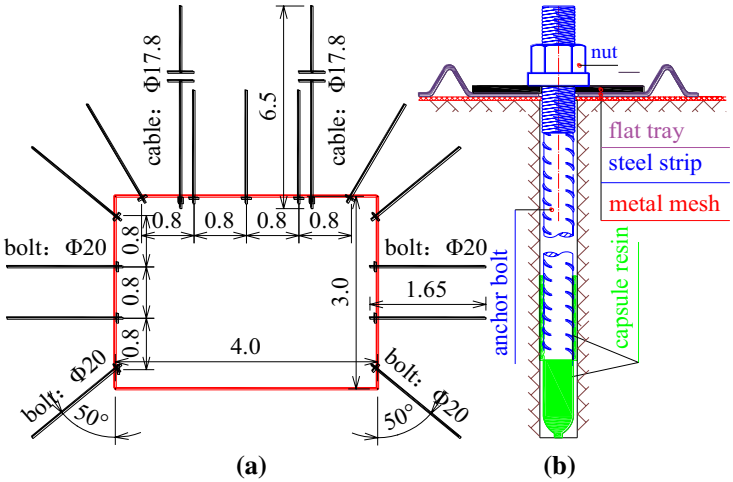

Fig. 1 The original support design of roadway: **a** support parameter of roadway; **b** structure of anchor bolt

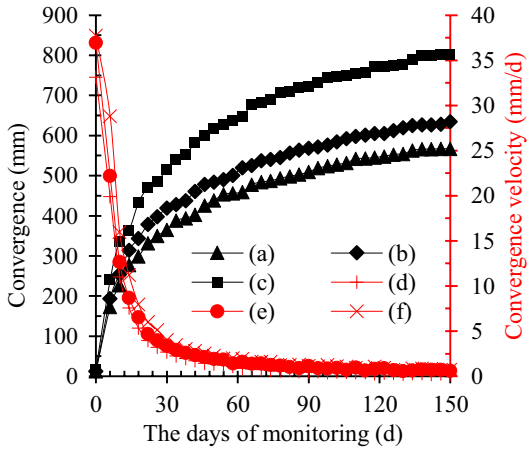

Fig. 2 The convergence amount and convergence speed of roadway section: (a) the convergence curve of two sides of roadway; (b) the convergence curve of the floor; (c) the convergence curve of the roof and floor; (d) the convergence velocity curve of two sides of roadway; (e) the convergence velocity curve of the floor; and (f) the convergence velocity curve of the roof and floor

anchor cable was made up of 1 × 7 steel strands with high strength and low relaxation, and the diameter of the anchor cable was 17.8 mm. The length of the anchor cable was 6.5 m. Each anchor cable was provided with three capsule resins, and the pre-strength of anchor cable was 70 kN.

The convergence of roadway surrounding rock presents the basic characteristics of omnibearing, strong rheology and large deformation. The convergence amount and convergence speed of roadway section are shown in Fig. 2. In the early stage after the roadway was supported, the convergence velocity of two sides of was 33.15 mm/day, the convergence velocity of the floor was 36.96 mm/day, and the convergence velocity between the roof and floor was 37.77 mm/day. Similarly, after supporting 150 days, the convergence of two sides of roadway was 567 mm, the convergence velocity of two sides of roadway was decayed to 0.17 mm/day. The convergence of floor was 635 mm, and the convergence velocity of floor was deteriorated to 0.61 mm/day. Furthermore, the convergence of the roof and floor was 803 mm, and the convergence velocity of the roof and floor were decayed to 0.73 mm/day. The rheological characteristics and omnidirectional convergent situation of surrounding rock of the coal roadway were exhibited. Specifically, the convergence of the floor accounts for 79.08% of the convergence between the roof and floor.

3 Characteristic Analysis of Instability

3.1 Failure Analysis of Supporting Structure

The destruction of components makes the support load provided by the support structure significantly compromised. This phenomenon will make it difficult for the surrounding rock of roadway to maintain its integrity and stability and provide effective support. After frequent transformation, roadway instability and structural failure characteristics are shown in Fig. 3. To overcome the disadvantage of greater flexibility of the metal mesh, BHW-280-3.00 steel strip was added between the metal mesh and the flat pallet. Due to the low bending rigidity, the steel strip like the metal mesh was also folded seriously, and some of the steel strips were even torn by the pallet. It is an unfavorable factor for the support structure to form a large area of compression zone in the roadway surrounding rock and to maintain its bearing capacity and stability. The bolt often breaks with flat fracture and obvious necking, showing the typical characteristics of tensile fracture of plastic materials. Therefore, the deformation characteristics of the bending combination show that the tray resistance fails to adapt to the bearing capacity of the bar.

3.2 Loose Circle Observation

In Fig. 4, it can be observed from the borehole imaging of roof and side of the roadway, the surrounding rock is

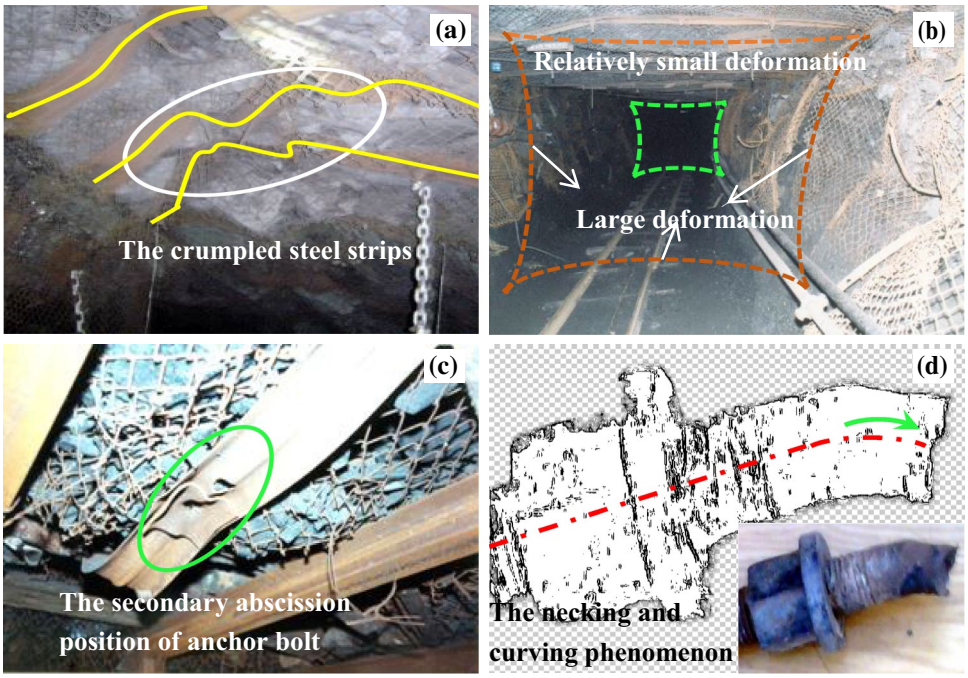

Fig. 3 Failure of the supporting structure: **a**folding phenomenon of steel strips; **b** deformation of roadway section; **c** secondary abscission position of anchor bolt; **d** necking and curving phenomenon of anchor bolt

extremely broken and the integrity of rock mass shows very poor.

Roof observation: the roof observation revealed that the longitudinal and transverse fractures were distributed within the range of 0–1.84 m, the circumferential fractures were mostly formed within the range of 1.84–3.42 m, and occurred intermittently within the range of 3.42–4.04 m. The fractures within the range of 4.04–7.24 m gradually transit from circumferential fissure to radial fissure. Simultaneously, the width of those cracks was in cm order of magnitude.

Rib observation: the roadway rib observation presents the coal body is enormously cracked within the range of 0–1.29 m, and the degree of broken was highest and serious borehole collapse was carried out. The coal body was broken within the range of 1.29–4.58 m, and have shown interlacing fractures. As the depth increases, the large-size sealing circumferential fractures appear intermittently, the coal body seemed with many separations, and the degree of damage of roof was significantly increased. However, the circumferential sealing fracture was mostly formed within the range of 4.58–7.58 m, and the fracture growth was large scale.

3.3 In-situ Stress Analysis

The calculated results show that the first principal stress is horizontal stress, the angle between direction and the roadway axis is 64.7°, and the measured peak value is 31.02 MPa. Similarly, the second principal stress is the self-weight of rock, and the measured peak value is 27.75 MPa. In addition, the third principal stress is also horizontal stress, the direction is 25.3° from the axis of the roadway, and the measured peak value is 14.27 MPa, as shown in Fig. 5a.

Generally, to reduce the effect of the stress field on roadway, the normal stress and vertical principal stress on the boundary of surrounding rock roadway should satisfy the following relationship, so that $\sigma_n = \sigma_v$ can be obtained as

$$\begin{cases} \sigma_n/\sigma_v = 1 \\ \sigma_n = \frac{1}{2}\left(\sigma_{H\max} + \sigma_{H\min}\right) - \frac{1}{2}\left(\sigma_{H\max} - \sigma_{H\min}\right)\cos 2\alpha \\ \alpha_0 = \frac{1}{2}\arccos\frac{\sigma_{H\max}+\sigma_{H\min}-2\sigma_v}{\sigma_{H\max}-\sigma_{H\min}} = 107.3^\circ \end{cases}. \quad (1)$$

Therefore, the roadway is simplified as a plane model perpendicular to the axis. Through the conformal transformation, the radial stress, circumpolar stress and tangential stress at any point in the surrounding rock of the roadway can be obtained as

$$\frac{\sigma_\rho - \sigma_\theta}{2} + i\tau_{\rho\theta} = \overline{\omega'(\zeta)}\frac{\varphi''(\zeta)\omega'(\zeta) - \varphi'(\zeta)\omega''(\zeta)}{[\omega'(\zeta)]^3}\zeta^2 + \frac{\psi'(\zeta)}{\omega'(\zeta)}\zeta^2, \quad (2)$$

$$\sigma_\theta - \sigma_\rho = 4\mathrm{Re}\frac{\varphi'(\zeta)}{\omega'(\zeta)}, \quad (3)$$

$$\varphi(\zeta) = \frac{\sigma_h + \sigma_v}{2}\eta\left[\frac{\zeta}{4} + \left(\frac{12\cos 2\alpha - 5\eta_1 - \eta_1^3}{28 - 4\eta_1^2} + i\frac{3\sin 2\alpha}{5 + \eta_1^2}\right)\zeta^{-1} + \frac{1 - \eta_1^2}{24}\zeta^{-3}\right], \quad (4)$$

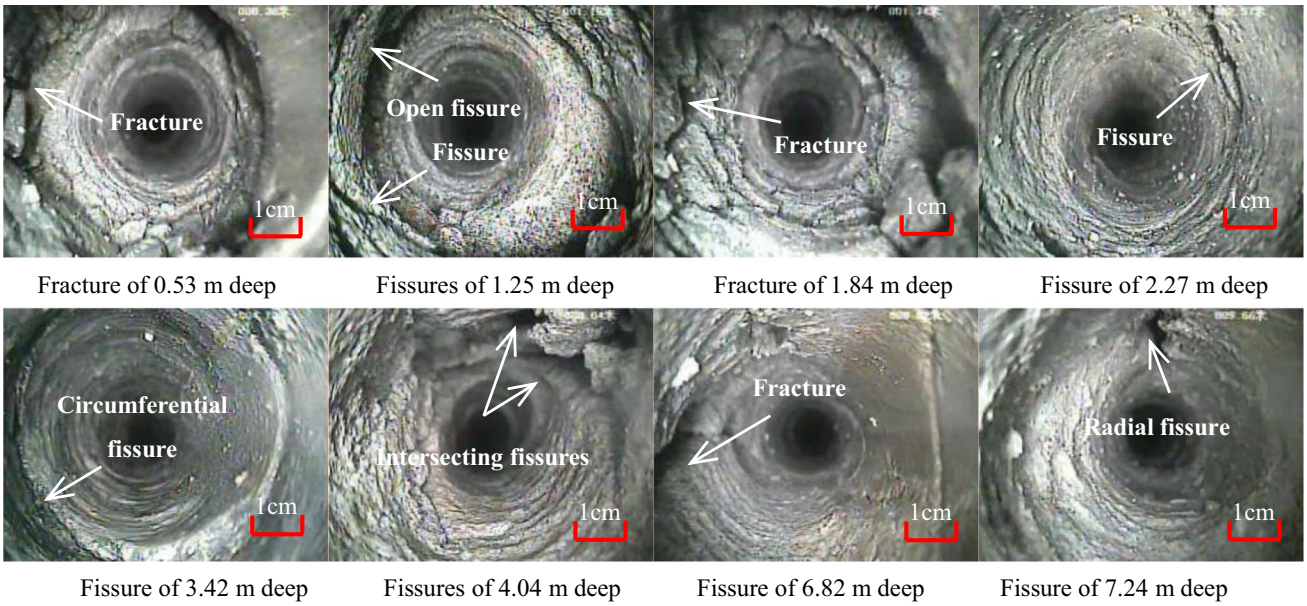

(a) Drilling in the roof strata

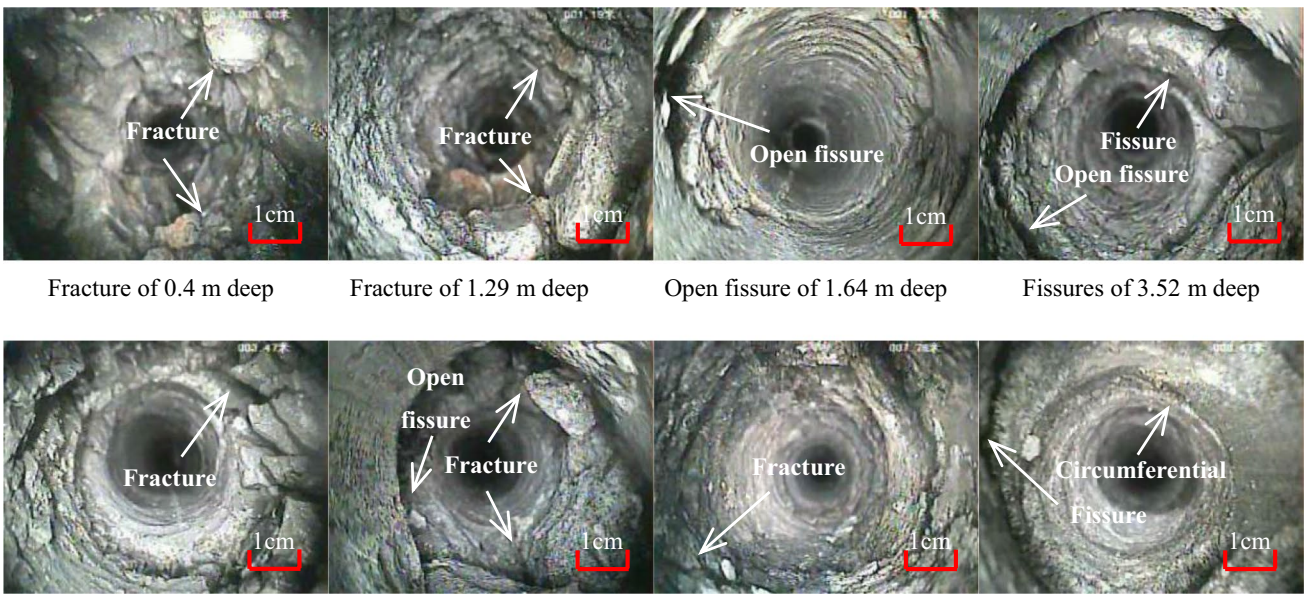

(b) Drilling in the ribs strata

Fig. 4 Fracture patterns of surrounding rocks from borehole TV observation

$$\psi(\zeta)=\frac{\sigma_h+\sigma_v}{2}\eta\left(\frac{\cos 2\alpha-\eta_1}{7-\eta_1^2}+i\frac{\sin 2\alpha}{5+\eta_1^2}\right)\times\frac{\left(\frac{1}{2}\eta_1^4-\eta_1^2+\frac{13}{2}\right)+(\eta_1^3-5\eta_1)\zeta^2}{1-\eta_1^2-2\eta_1\zeta^2+2\zeta^4}\zeta$$
$$-\frac{1}{2}\zeta^{-1}-\frac{e^{-2i\alpha}}{2}\zeta+\frac{1-\eta_1^2}{12}\times\frac{6+6\eta_1\zeta^2+\left(\eta_1^2-1\right)\zeta^4}{\zeta\left(1-\eta_1^2-2\eta_1\zeta^2+2\zeta^4\right)}, \tag{5}$$

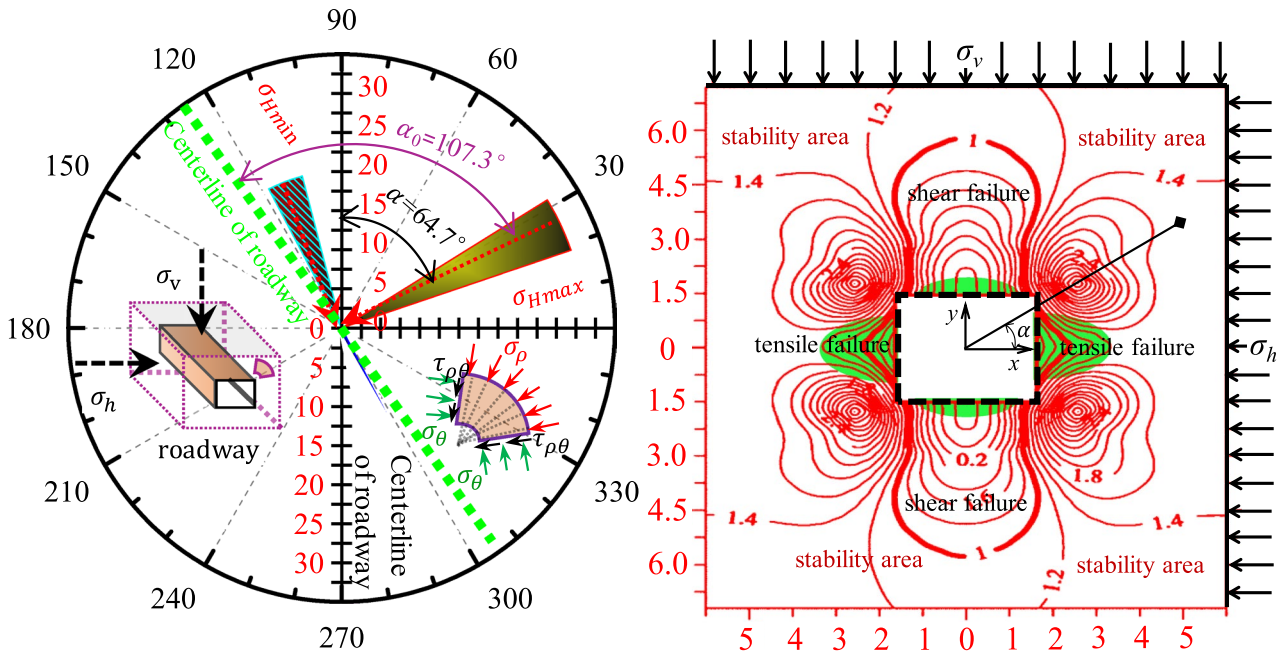

Fig. 5 **a** Azimuth relationship between the principal stress of the original rock and the axis of the roadway. **b** Failure type and regional division of roadway surrounding rock

$$\begin{cases} \omega(\zeta) = \eta\left(\zeta + \eta_1\zeta^{-1} - \frac{1-\eta_1^2}{6}\right)\zeta^{-3} \\ \eta_1 = \frac{-6(m+1)+4\sqrt{m^2+7m+1}}{2(m-1)} \\ \eta = 3H/\left(5+6\eta_1+\eta_1^2\right) \end{cases}, \tag{6}$$

where ζ is a coordinate function of a point in a complex plane, $\zeta = e^{i\theta}$, θ for the angle, σ_ρ for radial stress, σ_θ for circumferential stress, $\tau_{\rho\theta}$ for tangential stress, $\varphi(\zeta)$ for stress function, $\psi(\zeta)$ for stress function, η_1 for proportional constant, $m = H/L$, σ_h, σ_v are the horizontal stress and the vertical stress in the plane model, respectively. A is the angle between the radius and σ_h.

Substituting σ_ρ, σ_θ, $\tau_{\rho\theta}$ into the equation, respectively, the maximum principal stress at any point within the confining pressure σ_1 and minimum principal stress σ_2 :

$$\sigma_{1,3} = \frac{\sigma_\rho + \sigma_\theta}{2} \pm \sqrt{\left(\frac{\sigma_\rho - \sigma_\theta}{2}\right)^2 + \tau_{\rho\theta}^2}. \tag{7}$$

Combined with the Mohr–Coulomb criterion, set the safety factor as n, then

$$n = \left(\sigma_1 - \frac{1+\sin\varphi}{1-\sin\varphi}\sigma_3\right)/2\sigma_c\sqrt{\frac{1+\sin\varphi}{1-\sin\varphi}}. \tag{8}$$

When $n > 1$ indicates shear failure occurs in the rock mass, when $n = 1$ demonstrates the rock mass is in a critical state of shear failure,when $n < 1$ shear failure occurs in the rock mass. At the same time, $\sigma_1 > \sigma_t$ shows tensile failure occurs in the rock mass.

After the roadway was opened, the circumferential stress increases ranged from 60 to 90 MPa, and the radial stress unloading was about 30 MPa. The prominent contradiction between high-stress concentration and rock mass deterioration leads to rapid initiation, extension and penetration of fractures from the surface to the inside, rapid slide and expansion of rock mass skeleton, and increase the fracture damage speed and radius successively (Liu et al. 2016), Based on Fig. 5a, b, it is very clear to draw the following conclusions:

1. The influence of rock stress field on roadway direction is obvious (Huang et al. 2018a, b). The ideal roadway axis with $\sigma_{H\max}$, the angle should be 107.3°,and the axis of the actually arranged roadway $\sigma_{H\max}$ with the angle of 64.7°. This clearly denotes the unfavorable consequences for the control of surrounding rock roadway stability.
2. There are two failure modes of rock mass in the plastic zone of roof and floor: The superimposed zone of tensile failure and shear failure is within the depth range of 0–0.58 m in the middle part of the roadway. According to the borehole imaging tests,a large number of longitudinal and transverse fractures are distributed in this area,and the rock mass is relatively broken. The roof is in the range of 0.58–6.26 m depth and the principal failure mode of rock mass is shear failure.

3. There are two forms of damage in the two sets of plastic zone coal bodies: the depth ranged 0–1.73 m in the middle region of the two sides of the roadway is superimposed area of tensile failure and shear failure. According to the results of borehole imaging, in this region, the fractures are extremely developed in the coal body and seriously broken. In the range of 1.73–3.18 m depth, the actual failure mode of coal body is tensile failure. Thus, the theoretical prediction of tensile failure is in good agreement with the borehole consequences, which indicates the tensile failure is the major failure form of the coal body on the both sides of the roadway.

3.4 Coupling Analysis of the Failure Factors

Therefore, the nature of support failure was the combined result of high in-situ stress and the degradation of soft rock. The additional factors were like unreasonable arrangement of empirical support system and insufficient strength of structural materials. Given as following:

1. The supporting function of the bolt is to form effective axial compressive stress in the surrounding rock with its own tensile strength through the restraint of the tray, maintain the integrity of the rock mass, and improve the self-bearing capacity of the surrounding rock. In the original support scheme, the bolt material is 16Mn low-alloy high-strength structural steel with good ductility. However, the obvious necking phenomenon indicates that the bolt body still has the disadvantage of insufficient strength. At the same time, the bar body is clearly bent after fracture, and the fracture form caused by the combination of tensile bending indicates that the plate tray provides axial constraint to the bar body while applying a certain shear effect, resulting in the bending moment load, which makes it difficult for the plate tray to effectively adjust the bearing capacity of the rod.
2. The steel strip and metal mesh laid on the support section are all flexible constraints, and the limited transverse bearing capacity is difficult to form sufficient compressive stress on the roadway surface. Due to the strong displacement of the near-surface rock mass, folds and folds occur in many places of the steel strip and metal mesh. To make matters worse, because of the empirically rigid contact between the flat tray and the steel strip, this phenomenon will cause the flat tray tip to shear the steel strip or even tear it.
3. Bending and breaking of the bolt, folding and tearing of steel belt, folding of metal mesh, therefore, all these unfavorable factors could lead to the supporting structure difficult to provide enough support load. Also, it is difficult to form effective compression zone, forcing the crack expand extension. The existing achievements have further weakened the bearing capacity of the surrounding rock of the roadway, aggravated the strong convergence of the surrounding rock of the roadway, and promoted the further destruction of the supporting structure. Such chain reaction can only bring about the surrounding rock of the roadway. The possibility of instability has been further magnified.
4. The stress of the original rock is mainly tectonic stress. The prominent contradiction between high-stress concentration and degraded rock mass forms a large area of plastic zone in the surrounding rock of roadway. As a result, the end of the bolt is located in the shallow area where the vertical and horizontal cracks are connected, and the end of the anchor cable is located in the deep area where the large closed circumferential cracks occur. Therefore, it is difficult for the tension suspension function to be effectively exerted, which will make it difficult to guarantee the coordination of the primary and secondary bearing rings and realize the stability control of the roadway.
5. The calculated results show that the distribution of plastic zone of roof and floor is obviously symmetrical. However, the original plan did not take any support measures for the floor. Due to the limited bearing capacity of the broken rock mass and the crushing and swelling characteristics of the rock mass, it may be an adverse factor that causes the floor heave of the floor to be significantly larger than the roof subsidence. Based on the distribution characteristics of coal measures and borehole imaging, it is visibly risky to deal with the exposed floor.

4 Support Scheme and Simulation

4.1 Supporting Theory of Soft-Rock Roadway

To set the radius of loose circle in surrounding rock as $[r]$, and the critical strain of rock mass as $[\varepsilon]$, it can be inferred from the combination of Nishihara model and three-dimensional stress tensor as

$$[r]^2 = \frac{1}{2}\frac{a^2}{[\varepsilon]}(p_0 - p_\alpha)\left[\frac{\langle F\rangle}{\psi_2}t + \frac{1}{G_0} + \frac{1}{G_1}\left(1 - e^{-\frac{G_1}{\psi_1}t}\right)\right], \quad (9)$$

where a is the radius of roadway, p_0 is in-situ stress, p_α is supporting intensity, ψ_1 and ψ_2 are viscosity coefficient, t is time, G_1 and G_2 are shear modulus, and $\langle F\rangle$ is defined as

$$\langle F\rangle = \begin{cases} F & (F > 0) \\ 0 & (F \le 0) \end{cases}. \quad (10)$$

Based on Drucker–Prager criterion, F can be achieved as

$$F=\sqrt{3+\sin^3\varphi}\,\frac{\sqrt{3a^4\left(p_0-p_\alpha\right)^2+r^4(1-2\mu)^2p_0^2}}{r^2\left[2(1+\mu)p_0\sin\varphi+3\sigma_c\cos\varphi\right]}-1, \tag{11}$$

where φ is the internal friction angle, μ is the Poisson ratio, σ_c is a cohesive force and r is the depth of surrounding rock, $\langle F\rangle$ is the normal number of material yield under three-dimensional stress.

Figure 6 shows the mechanical effect of anchorage supporting in surrounding rock, the stress cones among the rods intersect to form a compression band.

From Eqs. (9), (10) and (11), the purpose of the support is to provide the sufficient support intensity (p_α) and contain the radius of loose circle (r) increments over time. According to the mechanical effect of anchorage support in the surrounding rock, the support strength p_α is obtained as

$$p_\alpha=\tan^2\left(45^\circ+\frac{\varphi}{2}\right)\times\frac{p^r+k\Delta u^r}{b\cdot s}\times d, \tag{12}$$

$$p=p^r+k\Delta u^r, \tag{13}$$

where b is bolt spacing, s is bolt row space, d is the thickness of compression band, p is the axial force of anchor bolt, p^r is pre-strength of anchor bolt, k is stiffness of anchor bolt and Δu^r is radial displacement of rock stratum. According to the analysis of soft-rock support theory, the new support system was adjusted as follows:

1. The symmetrical supporting system was arranged. The series of derivations (Eqs. 14, 15) expanded by Eq. (9) indicate that, under the soft-rock geology, particularly, the symmetrical distribution of the ground stress and coal bed, the symmetrical cross-section convergence appears. The asymmetric anchor network support system produces difficulty in achieving the stability control in deep soft-rock coal roadway.

$$u=\frac{1}{2}a\left(p_0-p_\alpha\right)\left[\frac{\langle F\rangle}{\psi_2}t+\frac{1}{G_0}+\frac{1}{G_1}\left(1-e^{-\frac{G_1}{\psi_1}t}\right)\right], \tag{14}$$

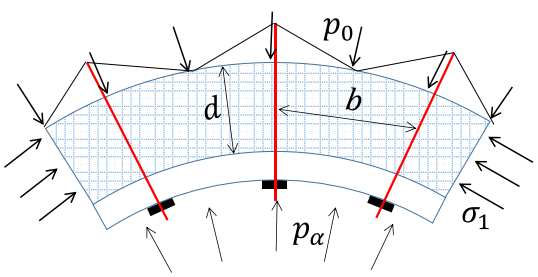

Fig. 6 The mechanical effect of anchorage support in surrounding rock

$$v=\frac{du}{dt}=\frac{1}{2}a\left(p_0-p_\alpha\right)\left[\frac{\langle F\rangle}{\psi_2}-\frac{1}{\psi_1}e^{-\frac{G_1}{\psi_1}t}\right]. \tag{15}$$

2. The instability process of the roadway surrounding rock is accompanied by the "Domino Effect" which is similar to the multi-factor coupling. The effective stress of surrounding rock is as shown in Eqs. (16) and (17). After the rock mass enters the yielding stage, the internal friction angle and cohesion force are linearly related to the strain of the rock mass, as shown in Eqs. (18) and (19). Therefore, when supporting the roadway, the supporting strength p_α of the supporting structure should be fully improved to ensure the effective stress of the roadway surrounding rock. In the same manner, reduce the softening degree of rock mass, enhance the cohesion and internal friction angle, to improve the inherent strength and deformation modulus of rock mass and restore normal stress of rock mass, limit the free surface and structural method to the expansion of the threshold, and prevent the further generation, extension and penetration of cracks in the surrounding rock mass.

$$\sigma_r^p=\frac{K_p'}{K_p'-1}\left[\frac{\left(K_p'-1\right)\sigma_r^e+2C'\sqrt{K_p'}}{\left(\frac{[r]}{r}\right)^{K_p'-1}}-2C'\sqrt{K_p'}\right]+2C'\sqrt{K_p'}, \tag{16}$$

$$K_p'=\left(1+\sin\varphi'\right)/\left(1-\sin\varphi'\right), \tag{17}$$

$$\begin{cases}\varphi'=\varphi-M_\varphi\times\left(\varepsilon-\varepsilon_e\right)\\ \sigma_c'=\sigma_c-M_C\times\left(\varepsilon-\varepsilon_e\right)\end{cases}, \tag{18}$$

$$\varepsilon=\frac{1}{2}\frac{a^2}{r^2}\left(p_0-p_\alpha\right)\left[\frac{\langle F\rangle}{\psi_2}t+\frac{1}{G_0}+\frac{1}{G_1}\left(1-e^{-\frac{G_1}{\psi_1}t}\right)\right], \tag{19}$$

where M_φ is friction angle softening modulus, M_C is viscosity-softening modulus, φ' is the residual angle of internal friction, σ_c' is residual cohesion, ε is a linear strain, ε_e is an elastic linear strain and σ_r^e is the effective radial stress of the elastic–plastic boundary surface.

It is necessary to decrease the softening degree of the rock mass, and improve the cohesion and friction angle. According to Eqs. (12) and (14), initially, the pre-strength p^r should be enhanced, the anchor bolt length L should be increased, the bolt spacing (b) and the bolt row space (s) should be decreased. Next, due to the positive correlation ($k\propto(EA/L_0)$), the elastic modulus E, and the anchorage area A should be increased. At the same time, low-alloy high-strength structural steel (Q500) has higher tensile

strength and good ductility ($\delta \geq 17\%$) can be used as the ideal material of bolt-bar.

3. The supporting efficiency of the combined supporting structure should be improved, and the stable state of the primary and secondary bearing ring should be effectively coordinated. Because of the fact $p_0 \ll p_\alpha$, to adapt to the requirements of support and deformation of the soft-rock coal roadway with high in-situ stress, the supporting structure in shallow should have high strength and ductility, the anchor cable should have a high strength to link up the shallow and deep rock masses effectively. Moreover, to improve the stress environment of the cone loose fracture rock mass between the anchor bolt and anchor cable, the contacting area of the supporting structure and the roadway surface should be increased.

4.2 New Support Design and Performance Test

1. As shown in Fig. 7, a scalable, high-performance extendable anchor bolt structure was taken with a diameter of 20 mm. The size of spherical tray was $150 \times 150 \times 10$ mm, and spherical height was 25 mm. The special-shaped tray was selected at the shoulder of a roadway, and the crush tube between nut and tray was applied with a height of 35 mm. A rubber blanket was rested between tray and steel strip, which measured $180 \times 180 \times 8$ mm, and it was made of the abandoned conveyor belt.

The ground mechanical properties of 3 groups with high-performance retractable anchor bolt indicated that the bearing capacity of the tail screw was 237 kN, 239 kN, and 240 kN with the elongation of 28%, 27%, and 27%, respectively. In the same manner, the bearing capacity of spherical tray was 220 kN, 218 kN, and 221 kN, correspondingly. The underground drawing experiment was conducted 30 min after the installation. When drawing force rises to 40 kN, the displacement of the anchor end was 0.5 mm. Similarly, when drawing force increases to 90 kN, the displacement of anchor end was 1.0 mm. Moreover, when drawing force rises to 210 kN, the anchor bolt was still in the elastic stage. The anchorage system (consist of anchor bolt, spherical tray, crush tube, nut) was well matched with the mechanical properties of anchoring agent.

2. The anchor cable was selected, that was made of 1×7 steel strands with low relaxation and high strength. The specifications of the anchor cable were as the type of lockset was KM18-1860, and the flat tray was made of $250 \times 250 \times 15$ mm steel plate. The U-shaped steel $16^{\#}$ was arranged between the lockset and metal mesh, which was no less than 600 mm. The eight groups of underground drawing experiments have shown that the breaking load and the elongation were 354–355 kN and 4.5–5.1%, respectively. Keeping in view the above scenario, the strength of anchor cable effectively meets support requirements.
3. The BHW-280-3.00 steel strip was set between the anchor bolt and the metal mesh. The metal mesh was placed on the full section of the roadway. Each anchor bolt was provided with three capsule resins, and the pre-strength of anchor bolt was 60 kN. Similarly, each anchor cable was provided with four capsule resins, and the pre-strength of anchor cable was 100 kN. The new support parameter of roadway is shown in Fig. 8.

4.3 FLAC^{3D} Simulation and Analysis

When establishing the roadway support model, the following assumptions are proposed for the model based on neglecting the secondary factors:

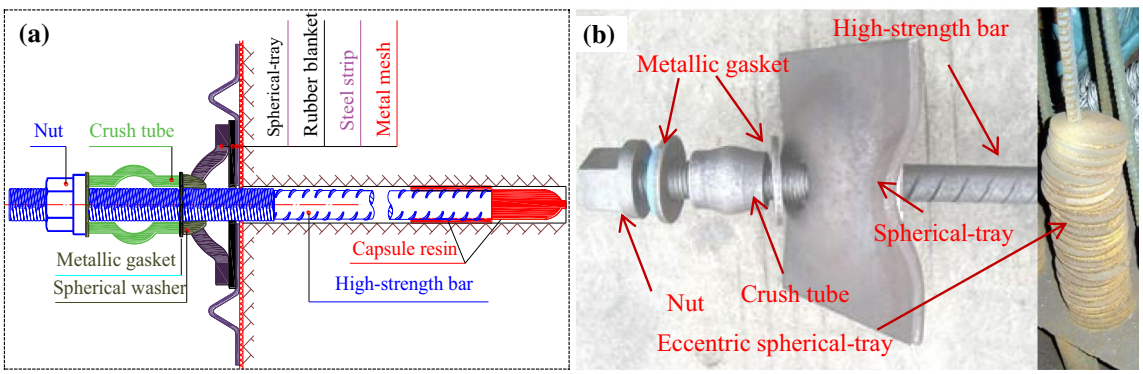

Fig. 7 The scalable, high-performance anchor bolt structure: **a** working condition of the scalable high-performance anchor bolt structure, **b** picture of real products of the scalable high-performance anchor bolt structure

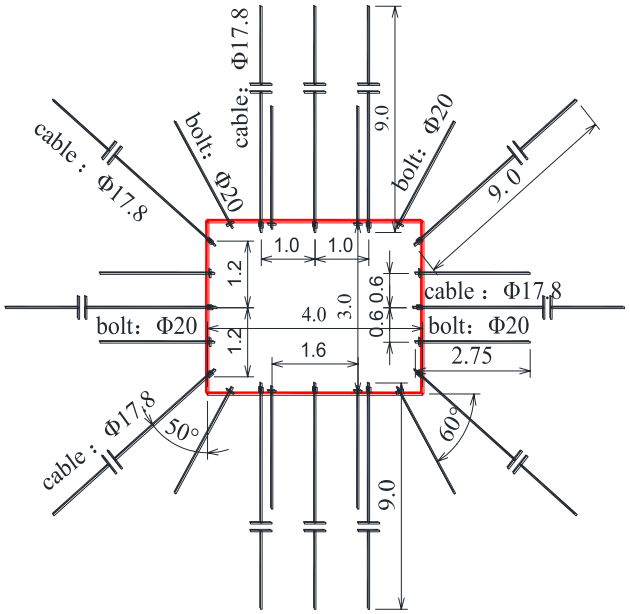

Fig. 8 The new support parameter of the soft-rock coal roadway

1. The influence of weak structural surface, joint fissure, fault structure, groundwater and other factors that may occur in actual projects was not considered.
2. The influence of additional stress and possible dynamic factors caused by surrounding rock deformation is not considered.
3. The calculation error caused by the possible distortion of the stress in the process of rock mass transmission is not considered.
4. The anchor rod is a continuous elastic homogeneous circular cross-section rod body. The anchorage agent and the rock mass bonded well. The anchor solid and surrounding rock mass are isotropic homogeneous elastoplastic materials, and the anchor solid and surrounding rock mass are isotropic homogeneous elastoplastic materials, which meet Mohr–Coulomb strength criterion.
5. The cumulative effects of axial tension, torsion, shear, bending and rock deformation before failure are ignored.

The roadway is horizontally arranged in the middle of the model. The roadway axis is parallel to the default y-axis in FLAC^{3D} software. At the same time, x × y × z = 40 m × 10 m × 37 m. During the simulation, in the z-axis direction, the normal displacement at the bottom of the model is locked as the bottom boundary condition, and the upper part of the model is a free boundary. The uniformly distributed load "σ" _"z" = 27.75" MPa is derived from the test data of the stress of the original rock. On the x-axis, the gradient function is "σ" _"x" = " ("35.15-0.025z") MPa by applying a gradually increasing normal stress as the boundary condition. In the y-axis direction, the gradual normal stress is also applied as the boundary condition. The gradual change function is "σ" _"y" = " ("26.16-0.025z") MPa. The engineering parameters are set according to Table 1.

Scheme 1: support shall be carried out according to the original design scheme, with row spacing between bolts of 0.8 × 0.8 m and row spacing between anchor cables of 2.0 × 0.8 m.

Scheme 2: except for the failure to install the 16# channel steel beam, the other support structure is the same as the new support scheme, which forms a support structure of "high-performance scalable bolt + low-relaxation high-strength anchor cable + metal mesh + steel strip + rubber gasket". Similar to the new support scheme, the row spacing between bolts is 0.6 × 1.0 m, and the pre-tightening force is 60 kN. The row spacing between anchor cables is 1.0 × 1.0 m, and the preload is 100 kN.

Scheme 3: Support according to the newly designed scheme to form a support structure of "scheme 2 +16#

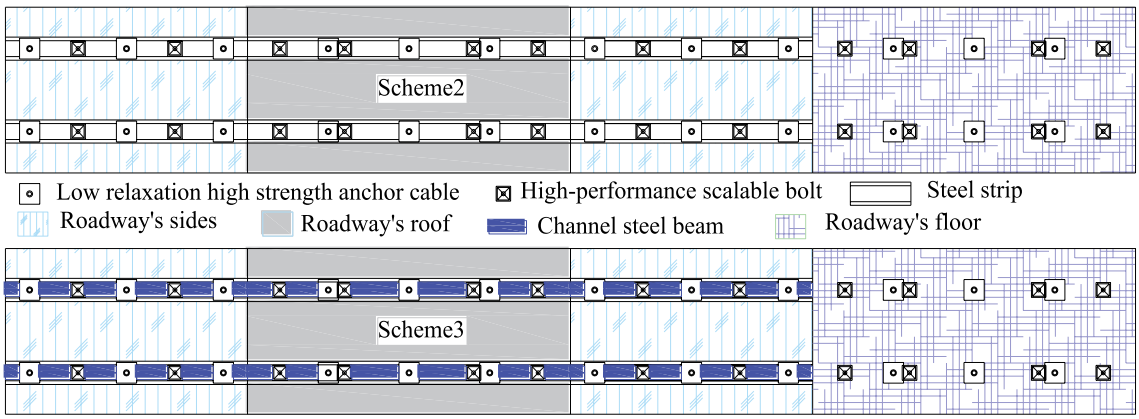

Fig. 9 The difference between scheme 2 and scheme 3

channel steel beam". The difference between scheme 2 and scheme 3 is shown in Fig. 9.

In the process of simulation, Mohr–Coulomb strength criterion is used to judge the failure of a rock mass. There are two kinds of observation points in the simulation: one is the four test points arranged on the roadway surface, which is used to observe the convergence of the roadway section; second, a test point is set at an interval of 0.5 m on the strike direction of the interface of rock strata to observe the subsidence of rock strata. Scope of coordinates of measuring points, respectively, is "10 × 20 or less or less", "y = 5.0", "z = 8.0/10.0/14/23/27/29". Simulation results of different schemes are shown in Fig. 10. The convergence amount and convergence speed of roadway section are shown in Fig. 11.

1. Since the two sides of roadway were arranged with a symmetrical supporting structure, including (scheme 1, scheme 2 and scheme 3), the horizontal stress was distributed symmetrically. For the scheme 1, as a result of the asymmetric support structure in the roof and floor, the vertical stress formed an asymmetric distribution. However, for the scheme 1 and scheme 2, because of the symmetrical distribution of the support system in the roof and floor, the stress distribution of roadway surrounding rock was symmetrical. According to this, the original design of the asymmetric support structure (scheme 1) was challenging to achieve the stability control of soft-rock coal roadway.
2. As compared with the original support design, the stress peak value was close to the roadway surface to differ-

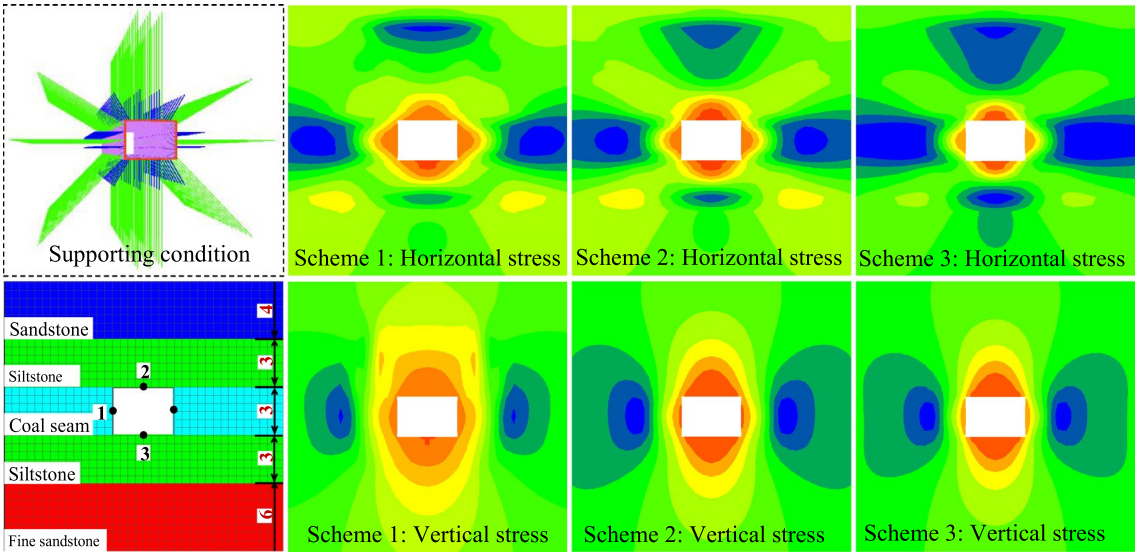

Fig. 10 Simulation results of different supporting schemes

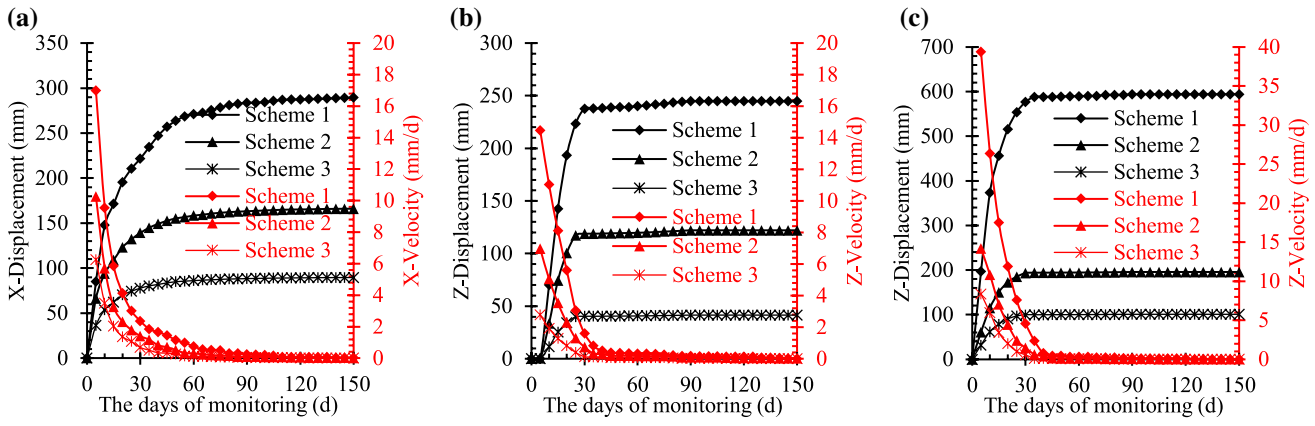

Fig. 11 Deformation of roadway: **a** X-Displacement of measure point 1; **b** Z-Displacement of measure point 2; **c** Z-Displacement of measure point 3

ent degrees under the new support function, irrespective of horizontal stress and vertical stress. The peak value of horizontal stress was 3.30 m, 2.67 m and 2.50 m away from roadway rib, and the peak value of vertical stress was 3.10 m, 2.68 m and 1.74 m away from the roof or floor with scheme 1, scheme 2 and scheme 3, respectively. The new support design can significantly improve the bearing capacity of roadway surrounding rock, especially the combination of 16# grooved steel beams and anchor cable. Therefore, the stressed environment of near-surface rock mass was optimized, and it was beneficial to improve the bearing capacity of the surrounding rock.

3. As shown in Fig. 12, at the beginning of supporting construction, the closure velocity of roadway rib was 6.25 mm/day, the floor bulging speed was 8.37 mm/day, and the closure velocity between roof and floor was 11.15 mm/day. After supporting 150 days, the convergence of roadway ribs was 179 mm, and velocity decays to 0.08 mm/day. The floor bulges to 100 mm, and velocity decays to 0.05 mm/day. The convergence of roof and floor was 142 mm, and velocity decays to 0.10 mm/day. Therefore, the cross-section of roadway has smaller convergence; the new support system maintains the stability of surrounding rock efficiently and effectively inhibits the extension of plastic zone.

5 Field Application and Result Analysis

The industrial field test was conducted in the haulage roadway with a length of 227 m. There were four monitoring points for the convergence of cross-sections arranged in the roadway, one monitoring point of anchor bolt (an anchor cable) for convergence observation (anchor bolt and anchor cable number are shown in Fig. 8). The interval of measurement points was 30 m, and the observations were recorded every 5 days. The cross-section convergence and the anchor bolt (anchor cable) stress monitoring points are as shown in Fig. 13.

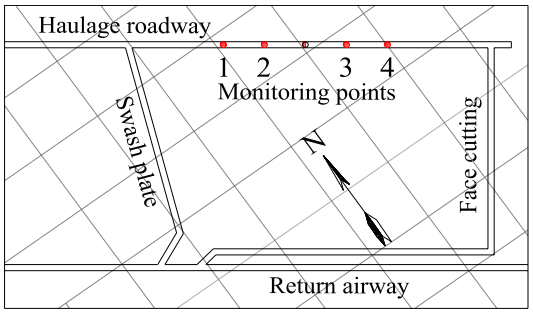

Fig. 13 The haulage roadway and monitoring points

5.1 The Stress Monitoring of Anchor Bolt and Anchor Cable

The stresses of anchor bolt in roadway ribs were maximum and almost equal. Similarly, the stresses of anchor bolt in roadway shoulder were approximately equal also. The stresses of anchor bolt in roof and floor were the lowest. The peak range of anchor shaft force was 88.15–134.80 kN, and the anchor bolt was still in a flexible stage, because the elastic limit was more significant than 210 kN. The shoulder cable was maximum, the stress of anchor cable in roof and roadway's sides were almost equal. The peak value range of anchor cable axial force was 169.59–241.29 kN. Comparing the breaking load of 364.8 kN, accounting for 46.49–66.16%, the condition of anchor cable was safe.

5.2 Crush Probability of Crush Tube

The crush probability of crush tube which was squashed in roadway rib, roof and roadway shoulder was 4.14%,

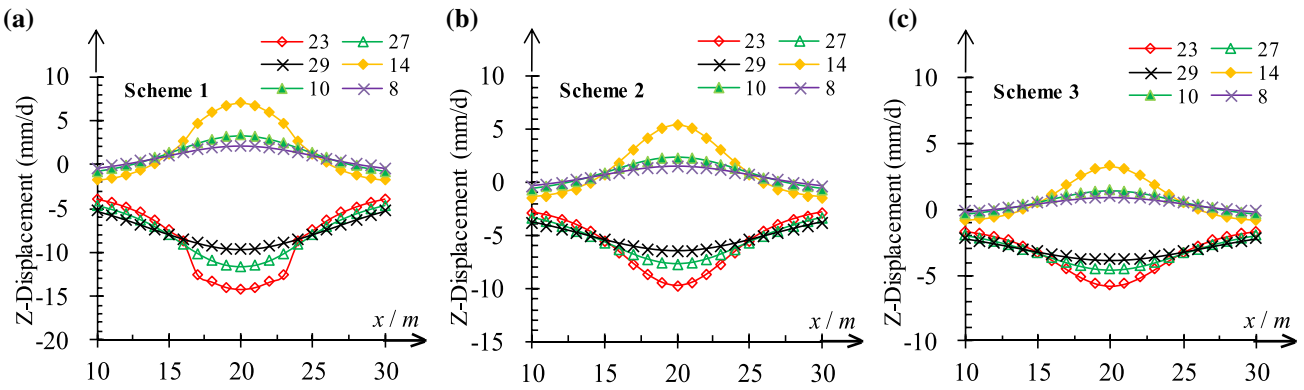

Fig. 12 Displacement of the surrounding rock: **a** Z-Displacement of surrounding rock of scheme 1; **b** Z-Displacement of surrounding rock of scheme 2; **c** Z-Displacement of surrounding rock of scheme 3

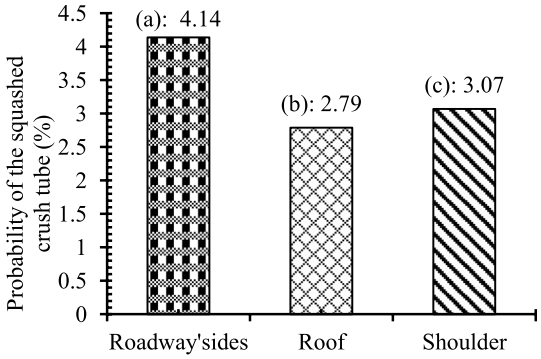

Fig. 14 Probability of the squashed crush tube: **a** probability of the squashed crush tube in two sides of roadway; **b** probability of the squashed crush tube in the roof; **c** probability of the squashed crush tube in roadway shoulder

2.79% and 3.07%, respectively. Furthermore, the total probability of the crush tube, which was compacted in the experiment of roadway was 10%, as shown in Fig. 14. Consequently, the choice of scalable, high-performance anchor bolt structure for the anchor system was significantly sound. It is necessary to add crush tube for anchor bolt. The extendable anchor system with high performance could release better effect, and to adapt to the large deformation support requirements of deep soft-rock coal roadway.

5.3 Cross-Sectional Convergence Monitoring

At the beginning of supporting construction, the surrounding rock still exposed strong rheological characteristics and omnidirectional convergent situation. The peak value of closure velocity of roadway ribs was 17.40–30.23 mm/day, which is decreased by 28.16%. Similarly, the peak value of the velocity of floor bulge was 19.20–21.66 mm/day that is decreased by 44.72%. Also, the peak value of convergence of roof and floor was 21.12–31.30 mm/day, decreased by 30.61%. After supporting 150 days, the convergence of roadway rib was 156.94–175.98 m that is decreased by 70.64%. The velocity of convergence decays to 0.03–0.10 mm/day, which is decreased by 61.76%. Furthermore, the peak value of floor bulge was 118.07–131.25 m, which is decreased by 80.37%. In the same manner, the velocity of floor bulge decays to 0.08–0.17 mm/day, which is decreased by 82.88%. After new support design was implemented, the convergence amount of roadway cross-section was significantly reduced, the converging rate of roadway was also suppressed effectively. The convergence amount and convergence speed of roadway section are shown in Fig. 15.

6 Conclusions

In this paper, through field experiments (including convergence test of roadway section + original rock stress test + borehole test), theoretical analysis and numerical simulation, the mechanism of instability of soft-rock coal roadway involving multi-factor coupling effect was analyzed. Based on the theoretical analysis of soft-rock roadway stability control, crush tube, spherical tray, high-strength bar and steel strip were organically combined for the new support structure. Studies have shown that:

1. The irrational design of the support scheme and the destruction of the support structure are the external causes of roadway instability. The destructive of the support structure is mainly reflected in the fact that the material strength is difficult to resist the high-stress environment of deep soft-rock roadway and the unreasonable matching of components is difficult to adapt to the convergence characteristics of soft-rock coal roadway. The deformation coordination of support components and the matching degree of bearing characteristics should be one of the main factors to be considered in the design of deep soft-rock roadway support.
2. The prominent contradiction between high in-situ stress environment and weak bearing capacity of deep degraded rock mass is the internal cause of roadway instability. The failure of the surrounding rock mass of the surrounding rock is mainly due to the dual effects of shearing and stretching. The degree of fracture of the coal and rock mass under the dual failure mode is significantly higher than that of the single form. The primary failure form of roof rock is a shear failure, and the primary failure form of two sides of coal is tensile failure.
3. The instability of roadway surrounding rock is accompanied by a "domino effect" similar to that of multi-factor coupling. Omnidirectional, strong rheology and large deformation convergence form the basic characteristics of deep soft-rock roadway deformation. Under the geological condition of soft-rock roadway with high ground stress, reasonable anchorage structure should have multiple characteristics of high strength, high elongation and adaptable. High strength is used to maintain confining pressure of surrounding rock mass. High elongation and adaptable are used to adapt to the basic characteristics of deep soft-rock coal roadway including omnidirectional, strong rheology and large deformation, adjust the bearing state of the bolt, and continuously provide effective constraints.

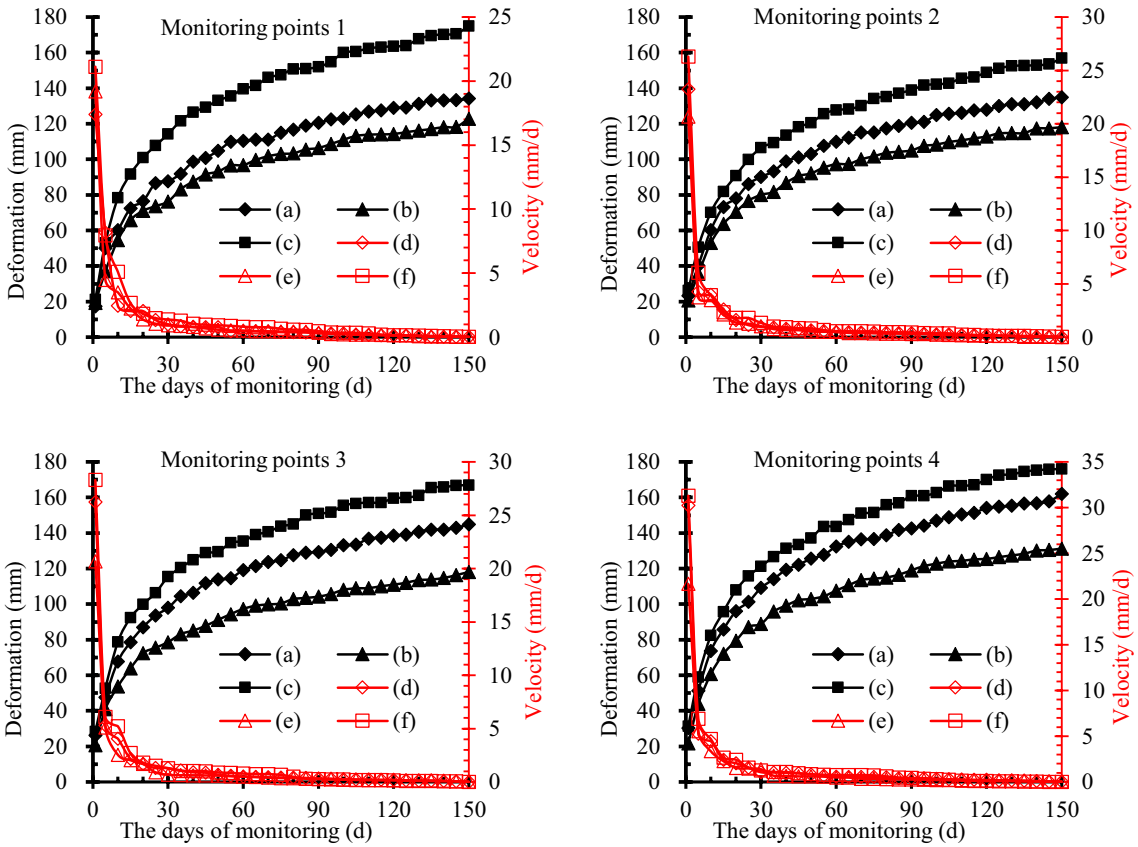

Fig. 15 The convergence amount and convergence velocity curves of roadway: **a** the convergence curve of two sides of roadway; **b** the convergence curve of the floor; **c** the convergence curve of the roof and floor; **d** the convergence velocity curve of two sides of roadway; **e** the convergence velocity curve of the floor; **f** the convergence velocity curve of the roof and floor

4. The newly designed support system (retractable high-performance anchor bolt + low-relaxation high-strength anchor cable +16# channel steel beam) comprehends the stability control of deep soft-rock coal roadway. The test results that the roadway section tends to be stable in a short time have shown that the coordination of the primary and secondary bearing rings effectively inhibits the convergence of the deep soft-rock coal roadway section. Besides, the crush tube failure ratio denotes that the bearing capacity of the bolt is effectively regulated. Consequently, by the organic combination of crush tube, spherical washer, spherical tray and rubber blanket, a new structural form can be provided for the stability control of deep soft-rock roadway.

Acknowledgements The research was funded by the National Natural Science Foundation of China (No.51574226), 2017 special project of Subject Frontiers Scientific Research in China University of Mining and Technology (2017XKQY047), and the National Natural Science Foundation of Guangdong (No. 2018A0303130162). The authors would like to thank Suncun Coal Mine for providing field geological and geotechnical data about this research, and for providing the encouragement to conduct this research and to publish the research findings.

Compliance with Ethical Standards

Conflict of interest The author declares no conflict of interest.

References

Aliha MRM, Bahmani A (2017) Rock fracture toughness study under mixed mode I/III loading. Rock Mech Rock Eng 50(7):1739–1751. https://doi.org/10.1007/s00603-017-1201-7

Aliha MRM, Sistaninia M, Smith DJ, Ayatollahi MR (2012) Geometry effects and statistical analysis of mode I fracture in guiting limestone. Int J Rock Mech Min Sci 51:128–135. https://doi.org/10.1016/j.ijrmms.2012.01.017

Ayatollahi MR, Aliha MRM (2004) Fracture parameters for a cracked semi-circular specimen. Int J Rock Mech Min Sci 41(3):356. https://doi.org/10.1016/j.ijrmms.2003.12.061

Ayatollahi M, Varasteh S (2017) Anti-plane interface cracks between two dissimilar orthotropic layers. J Phys: Conf Ser 843(1):12–13. https://doi.org/10.1088/1742-6596/843/1/012013

Ayatollahi MR, Karami J, Saboori B (2019) Mixed mode II/III fracture experiments on PMMA using a new test configuration. Eur

J Mech/A Solids 77:1–9. https://doi.org/10.1016/j.euromechsol.2019.103812
Colussi M, Berto F, Mori K, Narita F (2016) Effect of the loading rate on the brittle fracture of terfenol-d specimens in magnetic field: strain energy density approach. Strength Mater 48(6):791–800. https://doi.org/10.1007/s11223-017-9826-z
Erarslan N (2013) A study on the evaluation of the fracture process zone in ccnbd rock samples. Exp Mech 53(8):1475–1489. https://doi.org/10.1007/s11340-013-9750-5
Erarslan N, Williams DJ (2012) Investigating the effect of cyclic loading on the indirect tensile strength of rocks. Rock Mech Rock Eng 45(3):327–340. https://doi.org/10.1007/s00603-011-0209-7
Erarslan N, Alehossein H, Williams DJ (2014) Tensile fracture strength of brisbane tuff by static and cyclic loading tests. Rock Mech Rock Eng 47(4):1135–1151. https://doi.org/10.1007/s00603-013-0469-5
Feng X, Nong Z, He F, Yang S, Zheng X (2017) Implementation of a pretensioned, fully bonded, bolting system and its failure mechanism based on acoustic emission: a laboratorial and field study. Geotech Test J 40(6):978–999. https://doi.org/10.1520/GTJ20160157
Feng P, Dai F, Liu Y, Nuwen X, Zhao T (2018) Effects of strain rate on the mechanical and fracturing behaviors of rock-like specimens containing two unparallel fissures under uniaxial compression. Soil Dyn Earthq Eng 110:195–211. https://doi.org/10.1016/j.soildyn.2018.03.026
Frith R, Reed G, McKinnon M (2018) Fundamental principles of an effective reinforcing roof bolting strategy in horizontally layered roof strata and areas of potential improvement. Int J Mining Sci Technol 28(1):67–77. https://doi.org/10.1016/j.ijmst.2017.11.011
Ghamgosar M, Erarslan N (2016) Experimental and numerical studies on development of fracture process zone (FPZ) in rocks under cyclic and static loadings. Rock Mech Rock Eng 49(3):893–908. https://doi.org/10.1007/s00603-015-0793-z
Ghamgosar M, Erarslan N, Williams DJ (2017) Experimental investigation of fracture process zone in rocks damaged under cyclic loadings. Exp Mech 57(1):97–113. https://doi.org/10.1007/s11340-016-0216-4
Ghazvinian A, Nejati HR, Sarfarazi V, Hadei MR (2013) Mixed mode crack propagation in low brittle rock-like materials. Arab J Geosci 6(11):4435–4444. https://doi.org/10.1007/s12517-012-0681-8
Huang W, Wang X, Shen Y, Feng F, Wu K, Li C (2018a) Application of concrete—filled steel tubular columns in gob-side entry retaining under thick and hard roof stratum: a case study. Energy Sci Eng 018(00):1–14. https://doi.org/10.1002/ese3.442
Huang W, Yuan Q, Tan Y, Wang J, Liu G, Guang-long Q, Li C (2018b) An innovative support technology employing a concrete-filled steel tubular structure for a 1000-m-deep roadway in a high in situ stress field. Tunn Undergr Space Technol 73:26–36. https://doi.org/10.1016/j.tust
Kang H (2014) Support technologies for deep and complex roadways in underground coal mines: a review. Int J Coal Sci Technol 1(3):261–277. https://doi.org/10.1007/s40789-014-0043-0
Kang H, Wu Y, Gao F (2011) Deformation characteristics and reinforcement technology for entry subjected to mining-induced stresses. J Rock Mech Geotech Eng 3(3):207–219. https://doi.org/10.3724/SP.J.1235.2011.00207
Kang H, Yang J, Meng X (2015) Tests and analysis of mechanical behaviours of rock bolt components for China's coal mine roadways. J Rock Mech Geotech Eng 7:14–26. https://doi.org/10.1016/j.jrmge.2014.12.002
Liu Q, Yang K, Hua X, Li B (2016) In-situ stress measurement and its engineering application in deep coal mines: a case study in the Xinji Coalfield of China. J Eng Sci Technol Rev 9(6):59–68
Liu Y, Dai F, Nuwen X, Zhao T, Feng P (2018) Experimental and numerical investigation on the tensile fatigue properties of rocks using the cyclic flattened Brazilian disc method. Soil Dyn Earthq Eng 105:68–82. https://doi.org/10.1016/j.soildyn.2017.11.025
Lu Y, Wang L, Zhang B (2011) An experimental study of a yielding support for roadways constructed in deep broken soft rock under high stress. Mining Sci Technol 21(6):839–844. https://doi.org/10.1016/j.mstc.2011.05.034
Nazerigivi A, Nejati HR, Ghazvinian A, Najigivi A (2018) Effects of SiO_2 nanoparticles dispersion on concrete fracture toughness. Constr Build Mater 171:672–679. https://doi.org/10.1016/j.conbuildmat.2018.03.224
Serati M, Alehossein H, Erarslan N (2016) The brazilian disc test under a non-uniform contact pressure along its thickness. Rock Mech Rock Eng 49(4):1573–1577. https://doi.org/10.1007/s00603-015-0773-3
Shreedharan S, Kulatilake PHSW (2016) Discontinuum-equivalent continuum analysis of the stability of tunnels in a deep coal mine using the distinct element method. Rock Mech Rock Eng 49(5):1903–1922. https://doi.org/10.1007/s00603-015-0885-9
Song W, Liu X, Berto F (2018) Multiaxial fatigue crack orientation and early growth investigation considering the nonproportional loading. Phys Mesomech 21(4):358–370. https://doi.org/10.1134/S1029959918040100
Sun L (2015) Support failure of a high-stress soft-rock roadway in deep coal mine and the equalized yielding support technology: a case study. Int j Coal Sci Technol 2(4):279–286. https://doi.org/10.1007/s40789-015-0093-y
Tan Y, Yu F, Ning J, Zhao T (2015) Design and construction of entry retaining wall along a gob side under hard roof stratum. Int J Rock Mech Min Sci 77:115–121. https://doi.org/10.1016/j.ijrmms.2015.03.025
Wang H, Zheng P, Zhao W, Tian H (2018) Application of a combined supporting technology with U-shaped steel support and anchor-grouting to surrounding soft rock reinforcement in roadway. J Central South Univ 25(5):1240–1250. https://doi.org/10.1007/s11771-018-3821-9
Xu Y, Dai F (2017) Dynamic response and failure mechanism of brittle rocks under combined compression-shear loading experiments. Rock Mech Rock Eng 51(3):747–764. https://doi.org/10.1007/s00603-017-1364-2
Yang Y, Li H (2012) Failure mechanism of large-diameter shield tunnels and its effects on ground surface settlements. J Central South Univ 19:2958–2965. https://doi.org/10.1007/s11771-012-1364-z
Yu W, Wang W, Chen X, Du S (2015) Field investigations of high stress soft surrounding rocks and deformation control. J Rock Mech Geotech Eng 4:421–433. https://doi.org/10.1016/j.jrmge.2015.03.014
Yu W, Wu G, An B (2016) Investigations of support failure and combined support for soft and fractured coal-rock tunnel in tectonic belt. Geotech Geol Eng 36(6):3911–3929. https://doi.org/10.1007/s10706-018-0582-z
Zhang G, He F, Lai Y, Jia H (2018) Ground stability of underground gateroad with 1 km burial depth: a case study from Xingdong coal mine, China. J Central South Univ 25(6):1386–1398. https://doi.org/10.1007/s11771-018-3834-4
Zhao J, Zhang Y (2017) Studies on rock failure of layered rock in underground mining-face and control techniques. Geomech Geophys Geo-Energy Geo-Resour 3(4):405–414. https://doi.org/10.1007/s40948-017-0068-0
Zheng X, Zhang L, Zhang N (2013) Pre-stressed anchorage function and evolution in the roof of rectangular roadway in deep mine. J China Univ Mining Technol 42(6):929–934. https://doi.org/10.13247/j.cnki.jcumt.2013.06.007
Zhu X, Ren Y (2019) Numerical Simulation Study on the Anchorage Mechanism of Yield Supporting in Deep Tunnel. Geotech Geol Eng 37(3):2091–2102. https://doi.org/10.1007/s1070